remote sensing

MDPI

Article

Joint Communication and Jamming System Design Based on Filter Bank Multicarrier Chirp Waveform: Using for Curvilinear Flight Scenario

Gaogao Liu [1,*], Wenbo Yang [1], Yuqian Bao [1], Youming Wang [2] and Peng Li [1]

[1] School of Electronic Engineering, Xidian University, Xi'an 710071, China
[2] Guangzhou Institute of Technology, Xidian University, Guangzhou 510555, China
* Correspondence: ggliu@xidian.edu.cn

Abstract: A joint communication jamming waveform is proposed in this study based on the FBMC-chirp. To increase the number of false targets in a single pulse period, the chirp signal is modulated to different subcarrier groups. Since the subcarriers of the FBMC-OQAM signal are orthogonal, the signals are naturally orthogonal. This allows the transmitter and receiver to be separated and achieve multiple false target jamming, allowing the CFAR threshold to be raised by about 20 dB and protecting the target from detection. The ratio of the frequency shift of the designed jamming signal to the frequency modulation depends on the delay time, making the joint signal more robust in response to jamming and resistant to frequency modulation. The use of intercepted radar signals allowed channel estimation, providing high-speed digital transmission while ensuring multi-false-target jamming. The simulation results show that the joint signal has jamming effects on the pulse Doppler radar. The proposed FBMC chirp joint waveform requires about 20 dB less jamming signal ratio than the existing method, and thus the energy saved can ensure the robust performance of the communication subsystem in the joint communication jamming system. The proposed system has excelled in communication rate and bit error rate performance, ensuring that instructions are accurately and completely transmitted while implementing effective jamming.

Keywords: joint communication and jamming; filter bank multicarrier (FBMC); FBMC chirp waveform; waveform design

Citation: Liu, G.; Yang, W.; Bao, Y.; Wang, Y.; Li, P. Joint Communication and Jamming System Design Based on Filter Bank Multicarrier Chirp Waveform: Using for Curvilinear Flight Scenario. *Remote Sens.* **2023**, *15*, 1239. https://doi.org/10.3390/rs15051239

Academic Editor: Stefano Tebaldini

Received: 26 December 2022
Revised: 5 February 2023
Accepted: 20 February 2023
Published: 23 February 2023

1. Introduction

With the exponential growth in the use of electronic equipment, spectrum resources are becoming increasingly scarce. As important frequency systems, radar and communication each occupy a large part of the spectrum resources and continue to penetrate into the traditional spectrum range of the other party. Therefore, the relationship between radar and communication systems, namely the frequency band sharing between the two, has attracted widespread attention [1]. The joint radar communication system (JRCS) is not only conducive to reducing the occupation of the spectrum and improving the utilization efficiency of spectrum resources, but also conducive to the reduction in sensor volume and the simplification of signal processing through the full cooperation between the two functions. In recent years, such joint systems have been widely used in both military and civilian applications [2,3].

The core implementation of JRCS has two main research directions. One is to multiplex two independent signals in the time domain, frequency domain, space domain, and code domain under the premise that the two systems do not interfere with each other [4–6]. References [7–13] cover the latest waveform multiplexing technology and scheme in recent years. In contrast, another research direction is to use a single spectrum shared transmission signal for simultaneous radar detection and data communication, that is, dual-functional radar communication (DFRC) [14]. Generally, in the former, it is difficult to eliminate

mutual interference between signals, so the joint system cannot significantly improve spectral efficiency. The difficulty of the latter research lies in balancing the performance indicators of radar and communication systems so that the resolution of radar is increased and the communication performance metrics such as bit error rate (BER) are also improved.

At present, the development of beyond 5G (B5G) communication systems is in full swing. However, at B5G frequencies, orthogonal frequency division multiplexing (OFDM) is challenged by several effects, pushing alternative modulation formats [15]. As a candidate waveform for 5G communication, the filter bank multicarrier (FBMC) waveform is shaped by a well-designed prototype filter [16] to make the sidelobe of the frequency domain subcarrier extremely low, thereby reducing the inter-carrier interference (ICI), relaxing the requirements of inter-carrier synchronization, and ensuring its better performance in synthetic aperture radar (SAR) and communication integrated channels [17]. At the same time, FBMC does not use the cyclic prefix (CP) to combat inter-symbol interference (ISI) and ICI, improving spectral efficiency and avoiding false target imaging.

In modern national defense development, to achieve self-security and ensure that own weapons work well, combat equipment usually uses multiple electronic countermeasures (ECMs), including stand-off supported jamming (SSJ) and self-defense jamming (SDJ). Various types of ECM jamming have been developed, classified as either suppressive or deceptive jamming [18,19]. Multi-false-target jamming is commonly used to generate deceptive jamming. The ECM system senses incoming radar signals and simulates the target echo to generate replicas capable of confusing radar, hindering the identification of true and false targets [20,21].

Joint communication and jamming guarantees the unity of the joint system, namely complete communication with friendly own targets while jamming enemy radar or communication equipment. The joint system's main challenge is designing a common waveform that improves the system's communication performance while maintaining its jamming capabilities or increases the jamming performance of the system while maintaining its communication capability.

However, few studies have explored the technology of joint communication jamming. Most have focused on the joint radar jamming system and JRCS, while some have examined the design of integrated shared waveforms for additional interference. Reference [22] proposed a jamming method based on intermittent sampling inverse order filling for generating leading false targets. Reference [23] analyzed the effects of noise convolution and radio frequency (RF) noise jamming on the shared signal target detection and communication functions and proposed a method to interfere with shared signals using noise convolution and RF noise. However, the paper only studied the anti-jamming capability of the shared signal and did not investigate the jamming capability of the shared signal. An integration signal waveform for joint communication jamming was proposed in [24], utilizing false target jamming to increase the detection threshold for a constant false alarm rate. It uses the delay superposition of multiple sets of frequency modulation (FM) slope mismatch jamming signals. By the modulation mapping of the communication data, linear frequency modulation (LFM) signals with different Doppler and FM slopes can carry bits of data, ensuring that the communication instruction is completed while carrying out effective jamming. We have summarized the major contributions related to the type of paper proposal in Table 1.

This paper uses the joint communication jamming system for a joint signal based on the FBMC chirp. This waveform can improve the transmission rate of communication information and interfere with the opponent's radar detection to protect our intended target. First, we propose modulating communication information to different symbols after grouping and coding with the intercepted radar signal. An offset quadrature amplitude modulation (OQAM) scheme is used to map a series of bits of data to complex symbols. Then, the Doppler estimation is performed using the modulated chirp signal, and the frequency bias is compensated. The jamming and communication signals are demodulated and separated orthogonally, which can then be used for subsequent radar jamming and to

assist the communication signal in achieving channel estimation. The major contributions of this paper are as follows:

Table 1. Research on the major contributions related to the type of paper proposal.

Category	Reference	Model	Main Contributions
Multiplex two independent signals in the time domain, frequency domain, space domain, and code domain	[7]	Radar-embedded communications on an intrapulse basis	An incident radar waveform is converted into one of K communication waveforms, each of which acts as a communication symbol
	[8]	Exploit OFDM waveforms to perform both radar and communication operations	Optimize the transmission power of different subcarriers and assign the same OFDM subcarriers to different communication receivers
	[10]	Joint radar and communication waveform	Hide digitally modulated communication information inside an LFM radar signal
	[12]	Joint monostatic and bistatic radar-communication systems via chaos-based frequency modulated	Pulse generated through a chaotic oscillator for broadband radar imaging; information embedded by chaotic shift keying in the pulse
Use a single spectrum shared transmission signal	[14]	Dual-functional radar-communication	Achieved by embedding communication signals into radar pulses
	[22]	Design of integrated shared waveforms for additional interference	Jamming method based on intermittent sampling inverse order filling for generating leading false targets
	[23]	Anti-jamming capability of the shared signal	Interfere with shared signals using noise convolution and RF noise
	[24]	Joint communication jamming	Integration signal waveform utilizing false target jamming to increase the detection threshold for constant false alarm rate

1. A novel signal model and application scenario are established, and a novel joint communication jamming signal based on the FBMC chirp is designed.
2. This paper discusses the constraints of the novel joint waveform and simulates the performance of the proposed waveform by studying common guidelines for jamming waveform design and the selection of prototype filters in communication systems.
3. The suppression effect of multi-false-target jamming of the FBMC chirp signal was verified, ensuring a low BER of the communication subsystem.
4. Feasibility was demonstrated by implementing the proposed approach on a software-defined radio (SDR) device.

The rest of the paper is organized as follows: Section 2 discusses the geometric scene configuration of this paper. Section 3 presents the FBMC chirp waveform design and discusses the joint communication and jamming scenario and subsystem processing. The constraints and evaluation indexes of the joint signal are explored in Section 4, and Section 5 discusses the parameters and results of the simulation scenario. Section 6 presents the feasibility assessment of the proposed joint system using SDR-based hardware implementation, and the research conclusions are summarized in Section 7.

2. Model Construction

The jamming object of the joint system is an incoming aircraft with a curved flight path, which may be in the track-and-search mode or the SAR imaging mode. The joint system above refers to the joint communication and jamming system mentioned in Figure 1, hereinafter referred to as the joint system. The communication object is the communi-

cation aircraft. If the jamming signal and communication signal are emitted separately, the jamming signal will affect the communication process because the jamming beam is quite wide. To ensure communication quality, designing a transmit waveform with data communication and jamming radar is a very urgent need for the joint system.

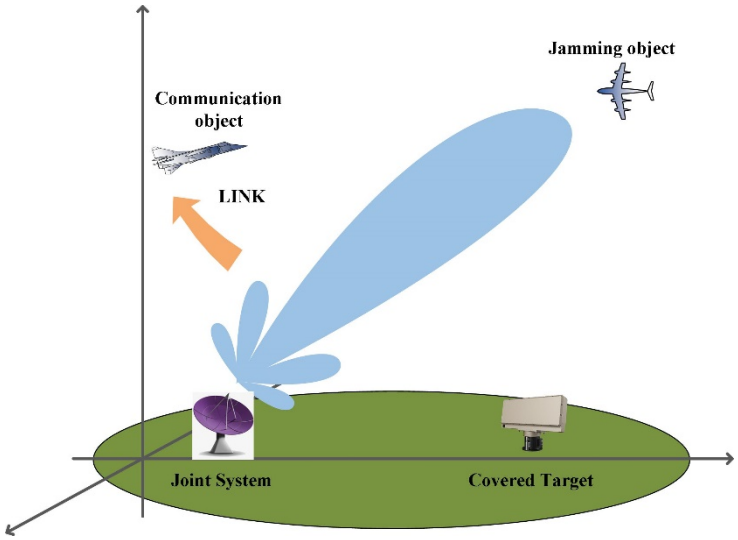

Figure 1. Application scenario of joint communication and jamming system.

A ground-based joint system (see Figure 1) senses radar signals of the incoming aircraft and generates replicas that simulate target echoes to confuse airborne radar, hindering it from identifying true targets from false ones and protecting the ground-covered target from jamming object detection. Meanwhile, the reconnaissance information is transmitted to the communication object. The communication object can judge the behavior of the incoming aircraft in real time and execute the function of uploading and sending commands according to the communication data. Because the communication task does not have high requirements on the direction of the antenna, the joint signal emitted from the sidelobe can still be received by the communication object and processed for communication.

3. Joint System Implementation

3.1. Filter Bank Multicarrier

Typically, information is transmitted through pulses that overlap in time and frequency in a multicarrier system [25]. The transmitted signal $s(t)$ of the time domain multicarrier system can be expressed as follows:

$$s(t) = \sum_{l=0}^{L-1} \sum_{k=0}^{K-1} g_{k,l}(t) x_{k,l} \tag{1}$$

where $x_{k,l}$ represents the transmitted symbol at subcarrier-position k and time-position l. $g_{k,l}(t)$ in Equation (1) is the transmitted basis pulse that is defined as follows:

$$g_{k,l}(t) = p(t - lT) e^{j2\pi kF(t-lT)} e^{j\theta_{k,l}} \tag{2}$$

and is a prototype filter $p(t)$ essentially, where F is the subcarrier interval, T is the time spacing, and $\theta_{k,l}$ is the phase shift. After transmission over the channel, the received symbols are decoded by projecting the received signal $r(t)$ onto the underlying pulse $g_{k,l}(t)$, such that

$$g_{k,l} = \langle r(t), g_{k,l}(t) \rangle = \int_{-\infty}^{\infty} r(t) g_{k,l}^{*}(t) dt \tag{3}$$

which corresponds to a matched filter in an additive white Gaussian noise (AWGN) channel.

Figure 2 shows the main differences between OFDM and FBMC, with an overlap factor $K = 4$ [26]. The former uses a rectangular window as the prototype pulse with a sinc function in the frequency domain sub-band with high partials, while the latter applies well-designed prototype filters with essentially no out-of-band leakage. PHYDYAS and Hermite prototype filters are discussed in more detail in Section 4.2. In addition, the good out-of-band suppression of the spectrum and the very high spectrum usage efficiency can make the jamming energy more concentrated in the main lobe and the jamming distance longer. These excellent properties allow FBMC to be used as an alternative signal for the joint communication and jamming system.

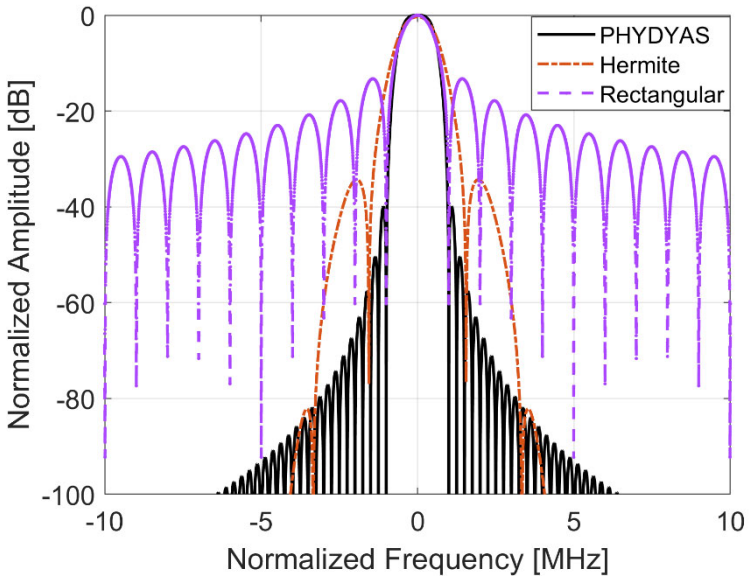

Figure 2. Comparison of three subcarrier prototype filters.

We introduce time representations for FBMC-QAM and FBMC-OQAM (see Figure 3). There is no single definition for FBMC-QAM. It either compromises on frequency localization or sacrifices orthogonality [27,28]. FBMC-OQAM, with the same symbol density as OFDM without CP, is related to FBMC-QAM. OQAM divides the complex signal of each subcarrier into two parts. A transmission delay of half a symbol period ($T/2$) is added so that the adjacent subcarrier interference is suppressed, ensuring that any subcarrier is orthogonal to its adjacent subcarriers while achieving full-rate transmission. Compared to OFDM transmitting complex signals, FBMC-OQAM transmits real-value signals on each subcarrier with half the coding efficiency of OFDM. However, the symbol rate of OQAM modulation is twice that of OFDM, so both signals' data rates are at the same level.

3.2. Joint Signal Design

OFDM chirp waveforms have been proposed in previous work [29–31]. Their basic principle is the separate modulation of the chirp signals onto different subcarrier groups. Since the OFDM signal subcarriers are orthogonal to each other, the signals on different subcarrier groups naturally satisfy orthogonality, so they can be separated at the transmitter and receiver ends, thus achieving multiple equivalents in the azimuthal direction. This allows the separation of the signals at the transmitter and receiver ends to form multiple equivalent phase centers in the azimuthal direction for high-resolution wide mapping band imaging.

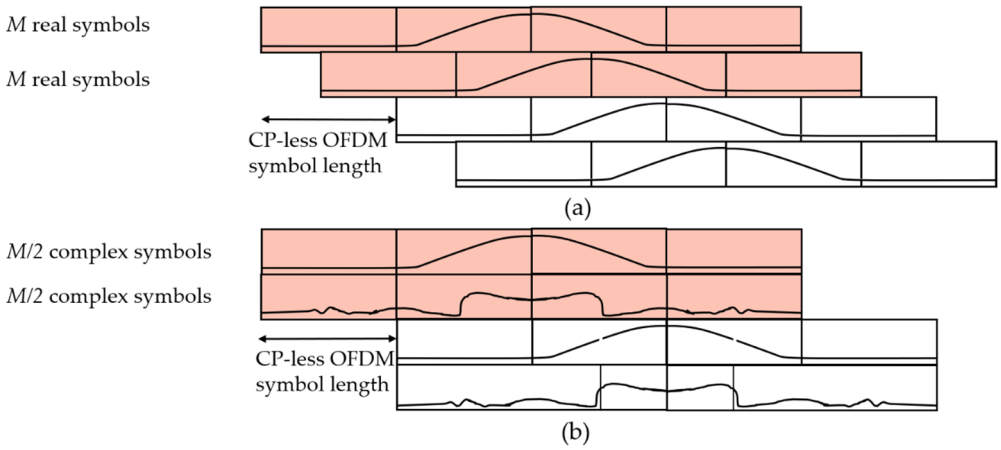

Figure 3. Comparison of time and frequency representations between FBMC-OQAM and FBMC-QAM waveforms: (**a**) FBMC-OQAM; (**b**) FBMC-QAM.

In this paper, to achieve the jamming function, we modulate the FBMC signal with a chirp signal, i.e., FBMC chirp signal. We propose an FBMC chirp signal with a generation matrix:

$$\mathbf{S} = \begin{bmatrix} \mathbf{s}(0,0) & \mathbf{s}(0,1) & \cdots & \mathbf{s}(0,M-1) \\ \mathbf{s}(1,0) & \mathbf{s}(1,1) & \cdots & \mathbf{s}(1,M-1) \\ \mathbf{s}(2,0) & \mathbf{s}(2,1) & \cdots & \mathbf{s}(2,M-1) \\ \vdots & \vdots & \ddots & \vdots \\ \mathbf{s}(M-1,0) & \mathbf{s}(M-1,1) & \cdots & \mathbf{s}(M-1,M-1) \end{bmatrix} \tag{4}$$

where $\mathbf{S}$ is the signal generation matrix, M denotes the number of quadrature signals, $\mathbf{s}(n,m) = \exp\{j\pi k_r t^2\} \times \exp\left\{n \cdot \frac{m \cdot j2\pi}{M}\right\}$, $t \in [0, T_r]$, n denotes the row index of the matrix, m denotes the column index of the matrix, T_r is the pulse width of the LFM signal, and k_r is the modulation frequency. When M quadrature signals are generated, the pulse width of the signal will be expanded to M times the original one. When the same LFM signal is modulated on each set of subcarriers, the number of false targets in a single pulse period can be increased to achieve multi-false-target jamming.

Taking the two orthogonal joint communication jamming signals as an example, the signal generation matrix is

$$\mathbf{S} = \begin{bmatrix} \mathbf{s}_1 & \mathbf{s}_1 \\ \mathbf{s}_2 \cdot e^{\frac{0 \cdot j2\pi}{2}} & \mathbf{s}_2 \cdot e^{\frac{1 \cdot j2\pi}{2}} \end{bmatrix} \tag{5}$$

where $\mathbf{s}_1$ is the communication signal to be modulated; $\mathbf{s}_1(t) = \sum_{i=1}^{N} c_i e^{j2\pi f_i t}$, where N represents the number of subcarriers, c_i represents the sub-band modulation weight, $C = \{c_i\}$ is the pseudo-random sequence of information encoding, and f_i is the ith sub-band carrier frequency. $\mathbf{s}_2$ is the designed multi-false-target jamming signal.

Jamming designs for radar can be divided into three categories [32–34]: non-coherent signal (e.g., noise jamming), fully coherent signal (e.g., forwarding jamming), and semi-coherent signal (e.g., frequency shift jamming). In this paper, we achieve the multi-false-target jamming mode with semi-coherent jamming by frequency shifting.

Assume the radar signal intercepted by the joint communication jamming system is a general chirp (also called LFM) signal $\mathbf{J}(t)$,

$$\mathbf{J}(t) = e^{j\pi k_r t^2}, \ -T_r/2 \le t \le T_r/2 \tag{6}$$

where T_r is the pulse width and k_r is the modulation slope. The intercepted radar signal is frequency-shifted and forwarded by the joint communication jamming system, which can be expressed as $\mathbf{J}_1(t) = e^{j\pi(k_r t^2 + 2\xi t)}$, where ξ is the frequency shift of the jamming signal.

The intercepted radar signal $\mathbf{J}(t)$ is truncated after a delay time τ, thus introducing the frequency-shifted term related to k_r

$$\mathbf{J}(t - n\tau) = e^{j\pi k_r t^2} \cdot e^{-j2n\pi k_r \tau t} \cdot e^{j\pi k_r (n\tau)^2} \tag{7}$$

where $n \geq 2$ and n is a positive integer.

Because of the fixed frequency-shift jamming $\mathbf{J}_1(t)$ after time-domain-matched filtering, the result can be calculated using Equation (8):

$$\begin{aligned} \mathbf{s}_{jout} &= \mathbf{J}_1(t) \otimes \mathbf{s}^*(-t) \\ &= \mathrm{rect}\left(1 - \tfrac{|t|}{T_r}\right) \sin c\left[\pi k_r T_r \left(t + \tfrac{\xi}{k_r}\right)\left(1 - \tfrac{|t|}{T_r}\right)\right] \cdot e^{j\pi\xi t} \end{aligned} \tag{8}$$

where $*$ is the conjugate operator, $\otimes$ denotes the convolution operator, and $\mathrm{rect}(\cdot)$ is a window function.

The maximum peak output after matched filtering of the jamming signal is at $-\frac{\xi}{k_r}$, which is shifted by $\frac{\xi}{k_r}$ from the moment of the real signal spike. When the FM slope k_r changes between the radar pulses, the false target will have a distance jump. If we want the false target to accumulate at the same distance, the shift (ξ) must be changed with the change in FM slope (k_r).

Therefore, the $\exp\left\{j\pi k_r (n\tau)^2\right\}$ term in Equation (7) needs to be further eliminated so that the first two terms in Equation (7) take the following form:

$$\begin{aligned} &\mathbf{J}(t - n\tau) \cdot (\mathbf{J}^*(t - \tau))^{n^2} \\ &= e^{j\pi k_r t^2} \cdot e^{-j2n\pi k_r \tau t} \cdot e^{j\pi k_r (n\tau)^2} \cdot (\mathbf{J}^*(t - \tau))^{n^2} \\ &= (\mathbf{J}^*(t))^{n^2 - 1} \cdot e^{j2\pi n(n-1)\tau k_r t} \end{aligned} \tag{9}$$

Multiply both sides of Equation (9) by $(\mathbf{J}(t))^{n^2}$ to obtain the jamming signal $\mathbf{s}_2(t)$:

$$\mathbf{s}_2(t) = \mathbf{J}(t) \cdot e^{j2\pi n(n-1)\tau k_r t} \tag{10}$$

where $-T_r/2 + n\tau \leq t \leq T_r/2$. From Equation (10), the ratio of the frequency shift ($\xi = n(n-1)\tau k_r$) to the modulation frequency (k_r) depends on the values of n and τ. The ratio of the shift (ξ) to the FM frequency (k_r) is a constant when n and τ take certain values in Equation (10).

The expressions for the communication signal and the radar jamming signal can be derived from the signal generation matrix:

$$\mathbf{s}_{com}(t) = \mathbf{s}_1(t) \cdot p\left(\frac{t}{\frac{T}{2}}\right) + \mathbf{s}_1(t - T/2) \cdot p\left(\frac{t - T/2}{\frac{T}{2}}\right) \tag{11}$$

$$\mathbf{s}_{jam}(t) = \mathbf{s}_2(t) \cdot p\left(\frac{t}{\frac{T}{2}}\right) - \mathbf{s}_2(t - T/2) \cdot p\left(\frac{t - T/2}{\frac{T}{2}}\right) \tag{12}$$

where t is the time width of one symbol of the joint signal, and $p(\cdot)$ is the PHYDYAS modulation prototype filter pulse function, received at the receiver end using the demodulation analysis pulse $p^H(t)$ and transposed conjugately with the prototype pulse. The FBMC system modulates the information on different carrier frequencies through this prototype filter. Transforming Equations (11) and (12) to the frequency domain, the frequency domain expression of the two quadrature signals can be obtained as

$$X_{\mathrm{com}}(2k) = \mathcal{F}\{s_1(n)\} \tag{13}$$

$$X_{\mathrm{jam}}(2k+1) = \mathcal{F}\left\{s_2(n) \cdot \exp\left(-j\frac{2\pi}{N}(n-1)\right)\right\} \tag{14}$$

where $s_1(n)$ is the sampling sequence that denotes the discrete time samples of a complex signal $\mathbf{s}_1(t)$ with the subcarrier length (N); $s_2(n)$ is the sampling sequence of $\mathbf{s}_2(t)$; $\mathcal{F}$ represents the discrete Fourier transform operator. The subcarrier interval Δf is F_S/N, and F_S is the sampling rate used for the discrete Fourier transform (DFT).

Adding the two signals gives a sign of the joint signal, and Figure 4 shows the frequency domain form of the joint signal. The multiplexing of the signal bands is achieved by dividing the available frequency band into several sub-bands, transmitting one signal in each sub-band, modulating the information to be transmitted to each subcarrier, and transmitting it simultaneously. The two orthogonal FBMC chirp waveforms are generated by zero interleaving and shifting a single chirp spectrum as the input sequence.

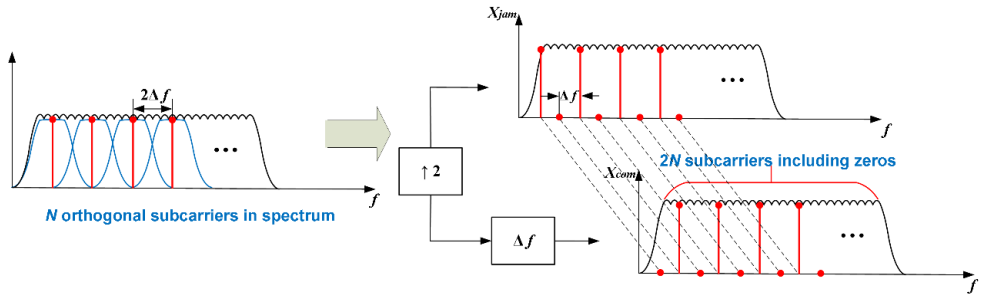

Figure 4. Symbol design of joint signal.

The proposed joint signal technique exploits the orthogonality of discrete frequency components, i.e., subcarriers. Assume the input sequence's spectrum is $X(k)$ with N discrete spectral components, separated by $2\Delta f$ (see Figure 4). The input sequence $X(k)$ is interleaved by N zeros, which is $X_{jam}(k)$ in Figure 4; then, the interleaved input sequence is shifted by Δf for the second data sequence $X_{com}(k)$. These data sequences are transformed into the time domain by the $2N$-point inverse discrete Fourier transform (IDFT). Finally, two waveforms modulated by the quadrature subcarrier set intershifted by Δf are obtained, and the demodulation process is realized by $2N$-point DFT. Note that both sets contain $2N$ subcarriers, but only N subcarriers are used to carry the input data.

Figure 1 shows the model considered in this paper. The joint system is ready for data communication based on achieving jamming to the incoming object. The functional trade-off is reflected in energy distribution for the joint signal designed with the orthogonal waveform regime. If the total transmit power remains the same, an increase in the energy of one of the signals will inevitably lead to a loss of energy of the other functional signal. In the joint waveform design, the communication signal energy mainly affects the BER, and the jamming signal energy mainly affects the jamming distance and jamming signal ratio (JSR). In the design, if the communication function is given priority, the energy resources can be more favorable to the communication signal; if the jamming effect is more important, more energy should be allocated to the jamming function.

3.3. Joint System Implementation

Figure 5 presents the proposed joint waveform method based on the FBMC chirp signal, where the communication information is first modulated to different symbols along with the intercepted radar signal after grouping and coding. A digital modulator is used to map a series of bits of data to complex symbols in light of the OQAM modulation scheme. Before transmittal to the RF front-end, its average value is removed and the power is normalized so that all emitted pulses have the same power. After the wireless transmission and jamming scenario, it reaches the receiver side. At the receiving end, the received signal is first symbol-segmented, and the signal is zeroed. The symbol sequence is converted to a bit sequence by synchronization, phase compensation, and then by a digital demodulator.

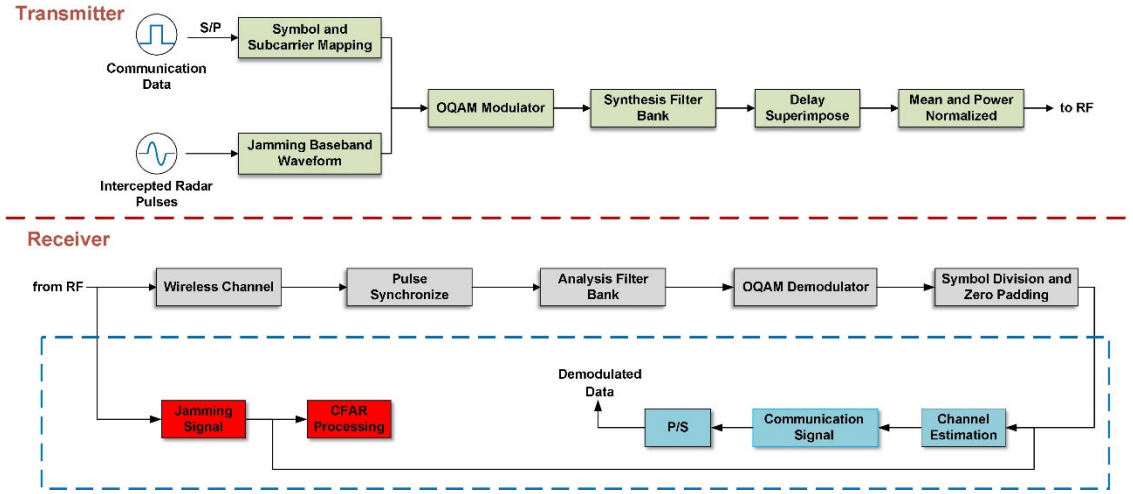

Figure 5. Joint communication and jamming system flow based on FBMC chirp signal.

Finally, after the channel decoding block that performs error correction while extracting uncoded bits are the protection remover and the parallel-to-serial (P/S) blocks. The jamming and communication signals are demodulated and separated orthogonally and can then be used for subsequent radar jamming and to assist the communication signal in achieving channel estimation, thus reconstructing different parallel branches of the original stream; finally, the collaborator's communication system recovers the original communication information.

The target reflected radar signal superimposed with jamming is the main component of the received waveform; therefore, it has to undergo standard radar processing. When radar carries out echo signal processing, it typically uses a constant false alarm rate (CFAR) detection algorithm to set the target detection threshold and compare it with the echo power to determine whether there is a real target. Specifically, CFAR can estimate clutter signal power in space by the noise, jamming, or ground clutter in several reference units around the target echo signal, and it can filter the noise signal and detect the target signal by setting the threshold after the clutter signal power change [35–37]. In addition, extended definitions for traditional CFAR, such as multi-static primary surveillance radar (MSPSR) and passive surveillance system (PSS) technologies, have been widely used in recent years and become the basis of surveillance [38].

Due to the presence of jamming signals in the reference units, the noise power estimated by CFAR is high, resulting in the detection threshold of CFAR being higher than the real target signal power, which achieves the coverage effect of the target. At the same time, due to the rise in the detection threshold of CFAR, the jamming signal is also lower than the detection threshold, so the opponent's radar cannot detect the jamming signal.

4. Extension to Constrained Designs

4.1. Design of Frequency Modulation Rate k_r

According to (6), the FM slope trimmed signal can be expressed as follows:

$$\tilde{\mathbf{J}}(t) = \exp\left[j\pi(k_r + \Delta k_r)t^2\right] \tag{15}$$

where k_r is the FM slope and Δk_r is the FM slope mismatch value.

Two FM slope signals are selected, corresponding to $k_{r1} = 0.9733k_r$ and $k_{r2} = 1.0274k_r$. Using the matched slope signals as reference signals, pulse compression is performed on these two signals, and the results are shown in Figure 6a. Zooming in on Figure 6a (see Figure 6b), the time width spreads widely, and the pulse compression output amplitude drops rapidly.

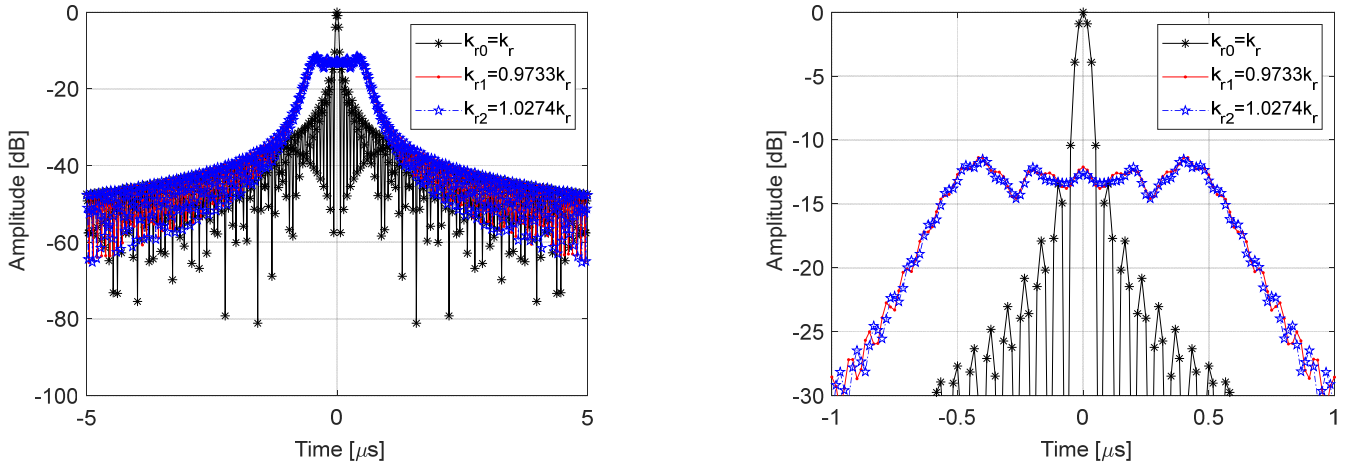

Figure 6. (**a**) Pulse compression results in different frequency modulation rates and (**b**) its zoom in results.

In Figure 7, the black dotted line shows the normalized peak and effective time width of the pulse compression output of the FM slope mismatch signal when the bandwidth is varied and the time width is 50 µs. When the bandwidth is 15 MHz and the time width is 50 µs, the signal is in the matched state. The peak of pulse compression is the highest, while the effective time width of the output is the smallest, forming an effective main lobe spike.

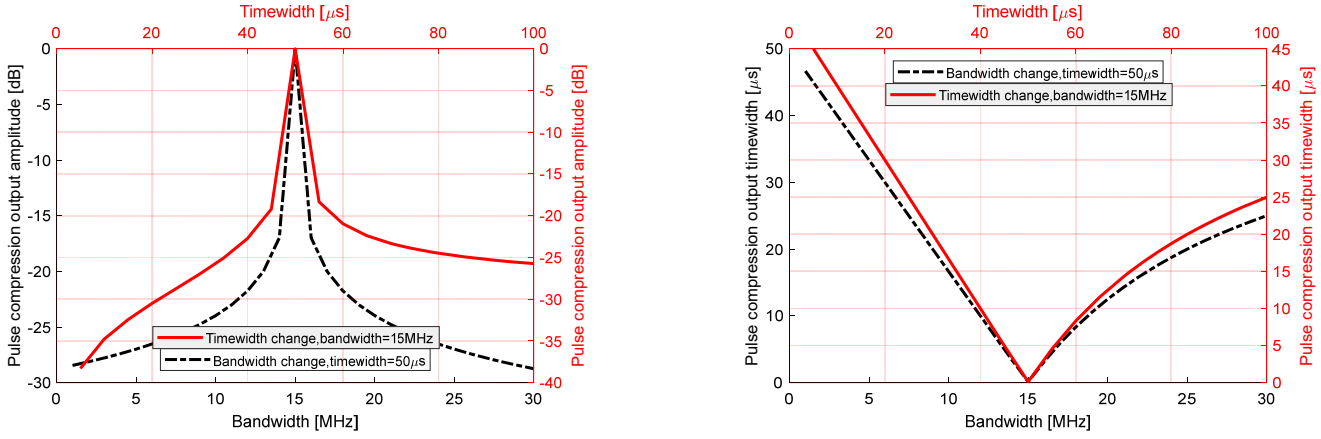

Figure 7. The effect of bandwidth change, time width = 50 us and time width change, bandwidth = 15 MHz on pulse compression output peak value (**a**) and effective time width (**b**) of FM rate mismatch signal.

The signal uses a multiple false target jamming style, which requires a chirp jamming signal, while the radar signal for the phase reference relationship requires that the tuning frequency does not mismatch to retain the pulse compression gain, i.e.,

$$\sqrt{|k_r|} \cdot T_r \geq \sqrt{BT_r} \tag{16}$$

4.2. Influence of Prototype Filter

This section discusses how different prototype filters can efficiently support the joint signal. According to the Balian–Low theorem [39], there are some fundamental limitations

in multicarrier systems that make it mathematically impossible to simultaneously satisfy the following desired properties:

1. Maximum symbol density $TF = 1$;
2. Time-localization $\sigma_t < \infty$;
3. Frequency-localization $\sigma_f < \infty$;

One of the prototype filters for FBMC-QAM is based on the Hermite polynomial [40], where the Hermite pulses have the same shape in time and frequency, allowing the symmetry to be exploited. Since the pulses are Gaussian-based and have a good joint time–frequency localization $\sigma_t\sigma_f = 1.02/4\pi$, almost as good as those obtained by Gaussian pulses ($\sigma_t\sigma_f \geq 1/4\pi \approx 0.08$), they are relatively robust in response to double-selected channels.

Another prominent filter is the PHYDYAS prototype filter [41]. Figure 8 shows the ambiguity functions of the above multicarrier prototype filters [42]; both PHYDYAS and Hermite filters are well localized in both time and frequency domains. Note that the Hermite filter is better localized in time than PHYDYAS but worse in frequency.

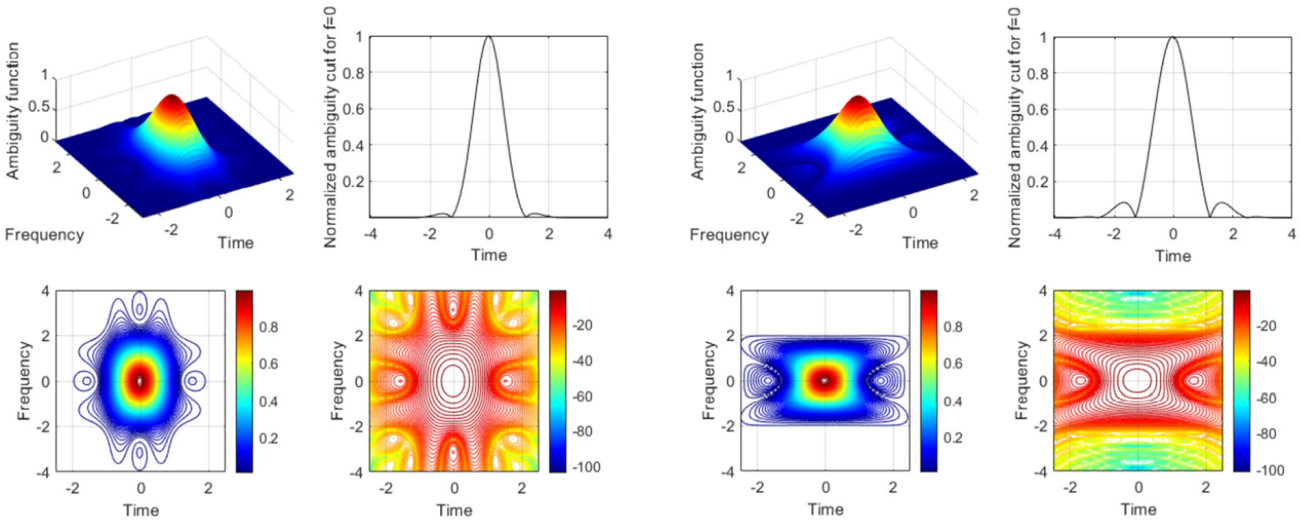

(**a**) (**b**)

Figure 8. Ambiguity function comparison of the Hermite (**a**) and PHYDYAS (**b**) prototype filters.

4.3. Minimum False Target SNR and Matching Gain Ratio

To improve the detection performance in multi-target environments, two types of constant false alarm detection methods are most commonly used: the mean constant false alarm detection proposed for noisy clutter environments and the ordered statistical constant false alarm rate (OS-CFAR) detection proposed for multi-target environments [43]. In general, the mean constant false alarm performs well in the background environment with constant noise and clutter boundaries, but its detection performance degrades significantly when multiple false targets are distributed on both sides of the target detection cell [44].

In this paper, we assume that the false alarm probability and the detection probability of OS-CFAR are known based on a priori detection information.

Assume that the joint communication jamming system does follow-team support jamming and is placed at a distance R_j from the radar signal emission direction. After the delayed partial forwarding by the joint system and the processing of the radar pulse compression and coherent accumulation, the signal-to-noise ratio (SNR) of the jamming signal be expressed as

$$JNR = \eta_i^2 \frac{P_{jt} G_{jt}^2 \lambda^2 \sigma}{(4\pi)^2 R_j^2 k T_0 B F L_j} \tag{17}$$

where P_{jt} is the jamming signal transmit power of the joint system; G_{jt} is the jamming antenna gain of the joint system; λ is the radar signal wavelength; σ is the radar scattering cross-sectional area of the target; k is the Boltzmann constant; F is the receiver noise factor; B is the signal bandwidth; T_0 is the effective noise temperature; L_j is the atmospheric loss and joint communication jamming system feed line loss.

Based on Equation (10), the ratio of the frequency shift ($\xi' = n(n-1)\tau k_r$) to the modulation frequency k_r depends on the n and τ. The ratio of the ith frequency-shifted jamming to the target echo matching filtering gain loss, η_i, is defined as follows:

$$\eta_i = 1 - n((n-i+1)! - (n-i)!)\tau/T_r \tag{18}$$

where $n!$ is the factorial function; n are positive integers, s.t. $n \geq 2$.

Using the known false alarm probability (P_{fa}), the minimum detectable probability ($P_{d\min}$), the radar-related parameters, and the minimum SNR required for the joint communication jamming system ($JNR_{\min}$), the corresponding matching gain ratio $\eta_{i\min}$ of the joint system can be found by substituting Equation (18).

4.4. Design of False Target Delay Interval $\Delta\tau$

In order to ensure the effect of jamming the radar, the delay interval $\Delta\tau$ of false target jamming must be designed. If the density of the false target is too large, the coherence and power of each false target signal will be reduced by superimposing each other, adversely affecting the interference effect.

From Equation (18), the greater the time delay, the greater the jamming matching filtering gain–loss ratio. The time delays for the positive and negative shifts of the target left and right are $\tau_1 = (1-\eta_1)T_r/n^2$ and $\tau_2 = (1-\eta_2)T_r/(n(n-1))$; the matching loss is greater for the overrunning false target compared with the lagging false target. The maximum time delays of the target's left and right positive and negative shifts are assumed to be $\tau_{1\max}$ and $\tau_{2\max}$, respectively.

Figure 9 shows the maximum time delays $\tau_{1\max}$ and $\tau_{2\max}$ when positive and negative frequency shifts are used for different positions to reduce the target detection probability to 0.1 in the process of the opposing radar approaching the protected target.

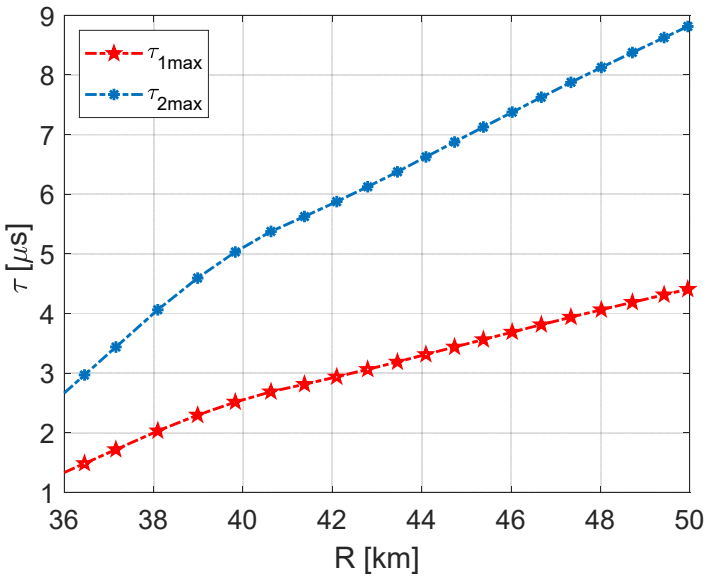

Figure 9. The maximum delay $\tau_{1\max}$ and $\tau_{2\max}$ at different positions when positive and negative frequency shifts are used.

The delay interval $\Delta\tau$ can be viewed as the communication element width, which affects the maximum communication rate of the joint system:

$$R_b = \frac{1}{\Delta\tau \cdot M} \cdot n_{bit} \tag{19}$$

where M is the number of pulse coherent accumulation of the intercepted radar. The digital modulator obtains the joint signal that maps the communication data to complex symbols according to the adopted OQAM modulation scheme, where a single symbol can carry n_{bit} data. The smaller $\Delta\tau$ is, the better the communication rate is.

4.5. Setting Number of False Targets

The multi-false-target jamming signal is formed by the superposition of multiple jamming signals with a delay, and its maximum delay should not exceed the pulse repetition period of the intercepted radar signal. So, the number of false targets is as follows:

$$J_M \leq PRT/\Delta\tau \tag{20}$$

5. Simulation Experiment Analysis

5.1. Experimental Settings

The simulation parameters of the joint signal and target are summarized in Tables 2 and 3. All simulations were performed on a standard laptop with Intel Core i9-12900H CPU 5.0 GHz, 16 GB RAM.

Table 2. Radar parameter configuration.

Parameters	Value
Pulse Repetition Time	1.5 ms
Band Width	15 MHz
Pulse Number	16
Pulse Width	50 us
Carrier Frequency	3 GHz
Target Velocity	20 m/s

Table 3. Joint system parameter configuration.

Parameters	Value
Overlapping Symbol	4
Simulation Length in Symbol	100
Bits per Subcarrier	2
Guard Bands on Both Sides	212
Signal Noise Rate	12 dB
FFT Points	1024
Jamming Distance Gap	100 m

The number of false targets was set to $J_M = 700$, distributed around the real target, to meet the jamming design requirements and make the signal jamming more easy and convenient. The parameter n in Equation (10) can be set to the smallest positive integer in advance; in this paper, n was set to 2. To see the jamming effect of our designed joint signal, we also simulated the opponent's radar in the scenario.

5.2. Communication Performance

For the jamming distance gap (see Table 3), we calculated that $\Delta\tau$ is 0.6667 μs, and the maximum number of false targets, calculated from Equation (20), was 2250. According to Equation (19) and OQAM modulation, the theoretical maximum bit rate of the system can be calculated as $R_b = \frac{1}{\Delta\tau \cdot M} \cdot n_{bit} = \frac{1}{2\times 100/3\times 10^8 \cdot 16} \cdot 200 = 18.75$ Mbps.

We compared the proposed waveform with the communication rate in [12]. Our proposed method performed better than the latter's communication data rate of 0.2 Mbps.

As discussed in Section 2, due to the complex target of the integration scenario, the received communication echoes have different time delays, and the integration platform will introduce multipath effects in the transmission process.

When the OFDM waveform has spectral leakage, it will form serious interference with the remaining subcarriers during spreading due to the serious out-of-band interference of its subcarriers, thus affecting the waveform orthogonality. FBMC has good out-of-band rejection; while using OQAM coding, it can equalize the subcarriers individually and avoid inter-subcarrier interference by using the analysis filter at the receiver side to achieve multipath rejection.

Figure 10 shows the communication performance of OFDM and FBMC waveforms in the presence of three paths. Figure 10a shows the BER at 150 m and 155 m with a three-path time delay, while the simulation results for the three-path delay of 2100 m and 2110 m are presented in Figure 10b. When the delay is exceeded, OFDM cannot suppress the multipath effect, and the BER cannot be reduced with increased SNR. The FBMC waveform is based on good out-of-band rejection, and inter-carrier interference is avoided by OQAM coding on subcarriers, which can effectively suppress the multipath phenomenon in combination with subcarrier equalization operation.

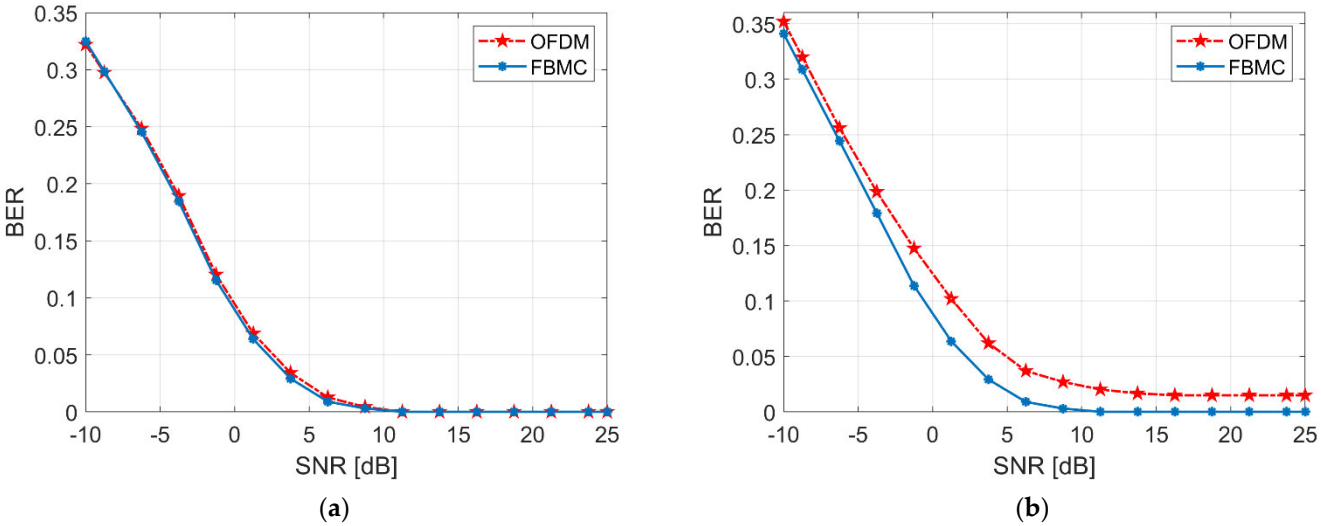

Figure 10. Comparison of communication performance under multipath delay (communication results with multipath delay less than CP (**a**) and communication results with multipath delay greater than CP (**b**)).

Figure 11 shows the communication transmission simulation results of the joint signal. The diamond-shaped line is the relationship between the communication BER and SNR estimated from an ideal Rayleigh channel, while the hexagonal line shows the worsened BER results for the OFDM waveform due to non-orthogonal factors (e.g., Doppler shift). The blue line shows the result of the FBMC chirp waveform. As the SNR increases, the channel estimation performance improves, and the BER gradually approaches the ideal value. However, the red and black lines show that channel estimation errors occur when the multipath delay exceeds the duration of one symbol, which leads to a sharp deterioration in the BER.

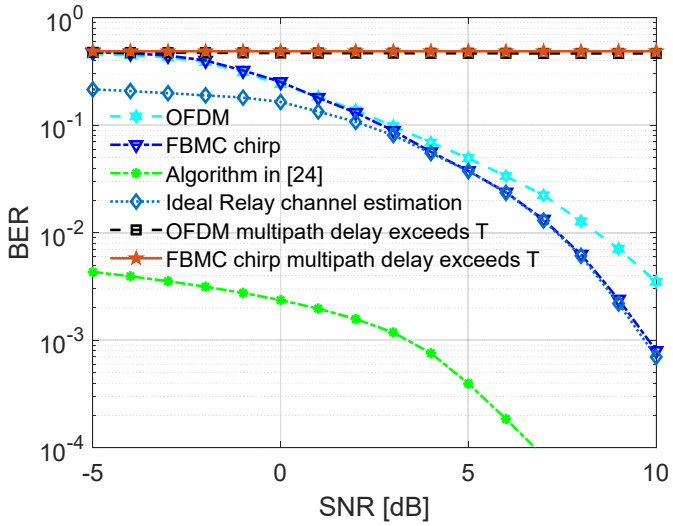

Figure 11. Simulation results of the joint system communication.

We then compared the proposed algorithm with the state-of-the-art algorithm presented in [24] (see Figure 11). The latter results in an improved signal-to-noise ratio after coherent accumulation due to the inclusion of the slow time-dimensional fast Fourier transform in its radar signal processing. When the green line (see Figure 11) input SNR is greater than 6 dB, the bit error rate drops to less than 10^{-4}. Without considering coherent accumulation processing, the proposed joint waveform does have a high bit error rate performance. This ensures that instructions are accurately and completely transmitted while implementing effective jamming.

5.3. Jamming Performance

Although the spectrum plot may look more crowded in practice for clarity, the spectrum plot of the proposed joint waveform with relatively few subcarriers (see Figure 12) shows that the jamming spectrum energy distribution is mainly concentrated in the main lobe. The main lobe spectrum of the jamming signal is relatively flat and shows a bump in the frequency domain with an approximate 15 MHz bandwidth. The dense false target jamming is spiky and can achieve the same spectral effect as the conventional comb-spectrum noise suppression type of jamming.

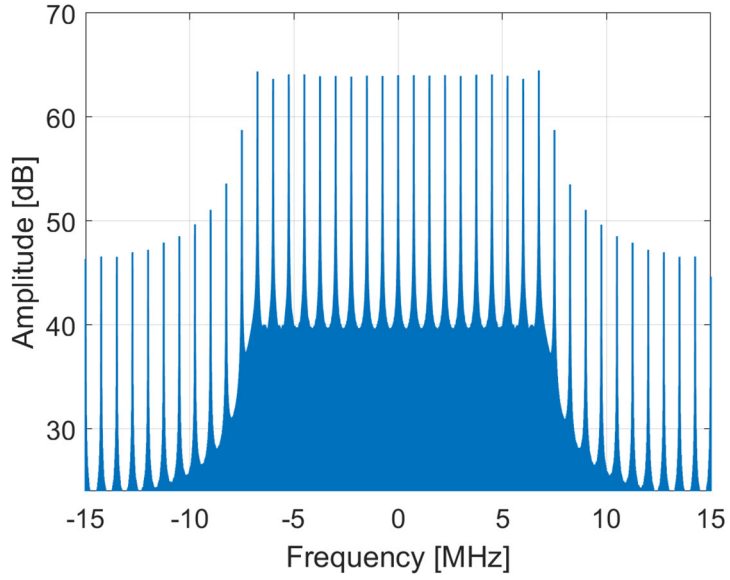

Figure 12. Spectrogram of the joint waveform based on FBMC chirp.

Figure 13a shows the results of the time–frequency analysis of the FBMC-chirp-based jamming signal with a Hamming window for the intercepted signal containing 16 radar pulses, which can be seen by taking one of the range lines and analyzing it in the time–frequency domain.

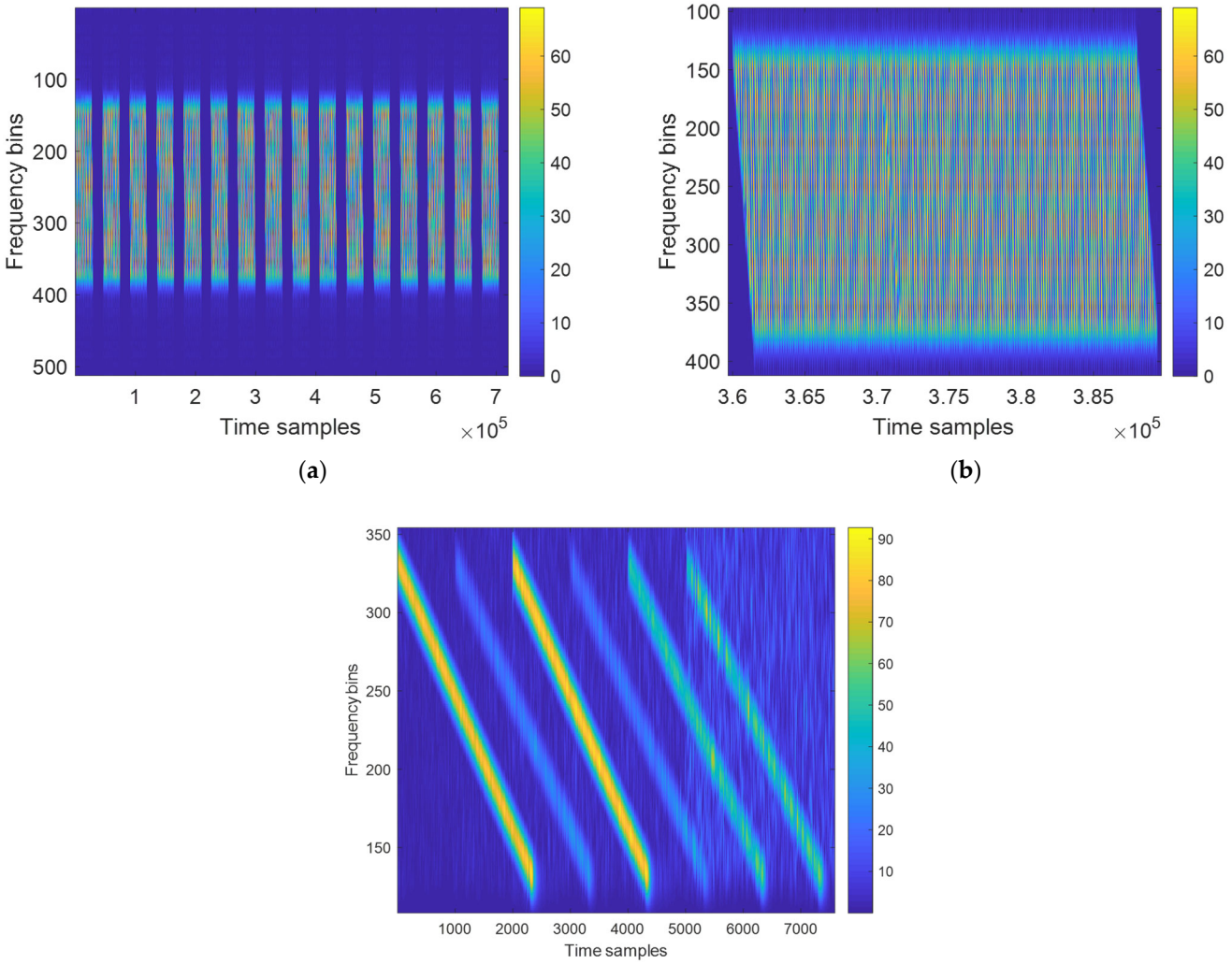

Figure 13. (**a**) Time–frequency analysis result of the FBMC chirp-based jamming signal; (**b**) the result with dense false target spacing; (**c**) the result with sparse false target spacing.

Figure 13b,c present the effect of time–frequency analysis of the interfering signal with dense and sparse false target spacings, respectively. The horizontal coordinates refer to the number of time sampling points, while the vertical coordinates represent the number of frequency points. As shown in the figures, the jamming signal designed in this study can be aimed at the frequency, and the frequency of the jamming signal varies linearly with time and lasts for the whole jamming cycle.

To verify the jamming performance of the joint system against the radar, a real target and jamming signals were set using the values in Tables 2 and 3. The results of processing echo signals with and without jamming are shown in Figure 14. In addition, we compared the proposed waveform with the state-of-the-art method in [24].

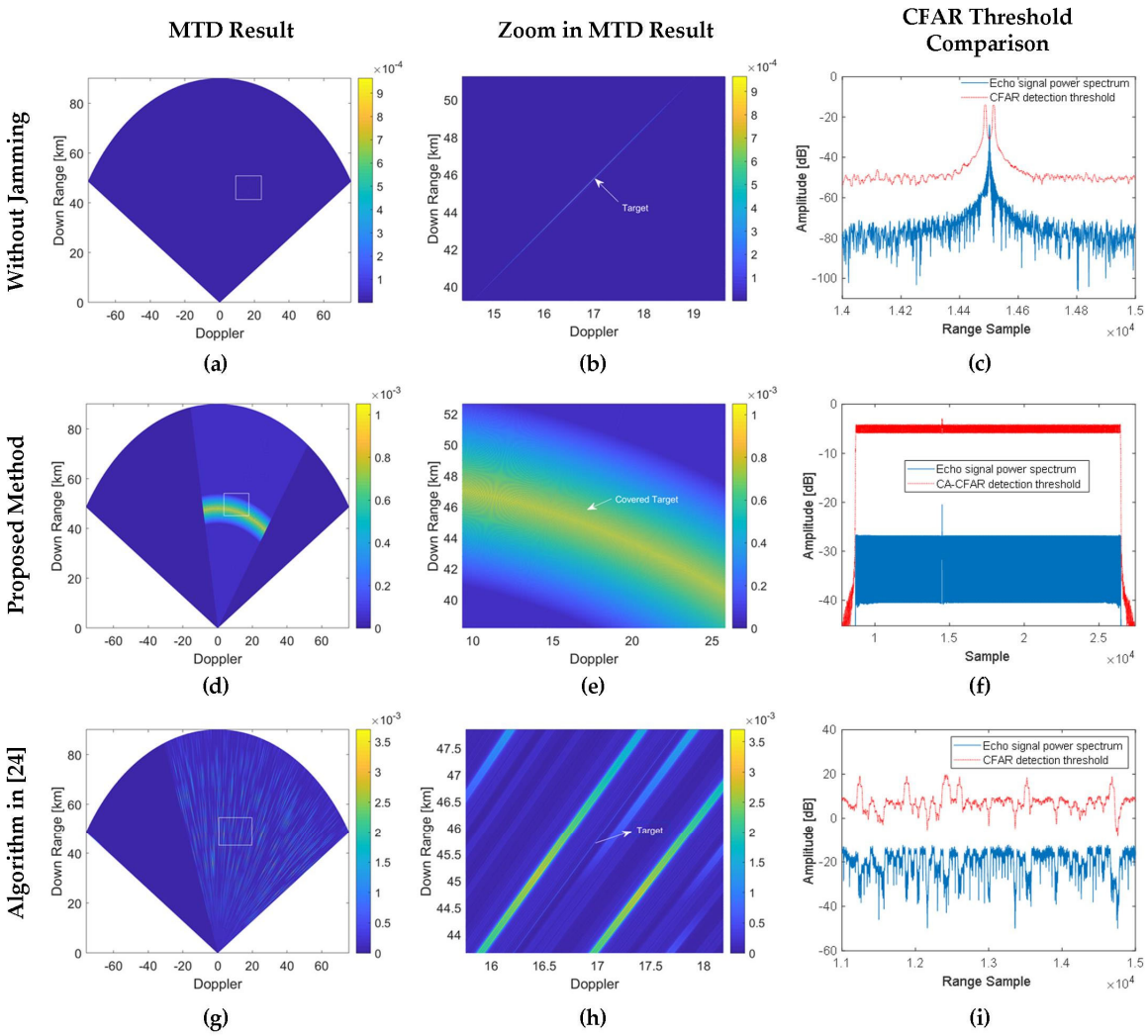

Figure 14. The results of multi-false-target jamming under the MTD and CFAR. The leftmost column (**a**,**d**,**g**) is the results of target echoes processed by MTD under three cases; the second column (**b**,**e**,**h**) is zoom in MTD results; the third column(**c**,**f**,**i**) is the comparison of CFAR threshold.

As shown in Figure 14, for the target echoes without jamming signals processed by moving target detection (MTD), the radar system was able to accurately detect the real target. When the jamming signal was included in the echo, the real target's echo was covered by the interfering signal. After MTD and CFAR processing, the opponent's radar system was unable to find the real target, with the jamming signal acting as a shield for the real target.

Because the FBMC spectrum has good out-of-band suppression, the proposed joint communication jamming signal has very high spectrum use efficiency by making the FBMC chirp jamming signal energy more concentrated in the main lobe, fully reducing the energy of the side lobe of the jamming signal. The radar system also cannot detect the covered target. The FBMC chirp requires less jamming power than chirp or other signals, which can save energy in the joint system and ensure the robustness of communication transmission quality.

The third column in Figure 14 illustrates the results of multi-false-target jamming on the threshold relationship of CFAR. Compared with the CFAR detection results of multi-false-target jamming in [24], the jamming signal of our design enters the reference cell of the radar's CFAR detector, increasing the estimated noise power of the CFAR detector. This results in a CFAR detection threshold of about 20 dB higher than the target signal power to achieve the coverage effect on the target. Due to the elevated threshold value of CFAR,

the jamming signal is also lower than the threshold, and the opponent's radar is unable to detect the jamming signal; thus, the coverage of the intended target is completed.

CFAR detection cannot avoid complex clutter and noise environments, so the hypothesis test for detecting the presence of objects in echo signals is uncertain. Thus, a measure of uncertainty, i.e., entropy is defined as follows:

$$E(x) = -\int_{-\infty}^{+\infty} p(x) \log_a p(x) dx \tag{21}$$

where p is the sum of FBMC subcarrier power distributed in the jamming frequency band.

Assuming that the interfered radar frequency band is known, the entropy in the interfered frequency band can be maximized to improve the jamming ability to achieve the best jamming effect. As shown in Figure 15, although the proposed joint communication jamming waveform is slightly lower in jamming entropy than the algorithm in [24], our proposed joint waveform requires less jamming power than traditional chirp or other signals. The energy saved can ensure the robust performance of the communication subsystem in the joint communication jamming system.

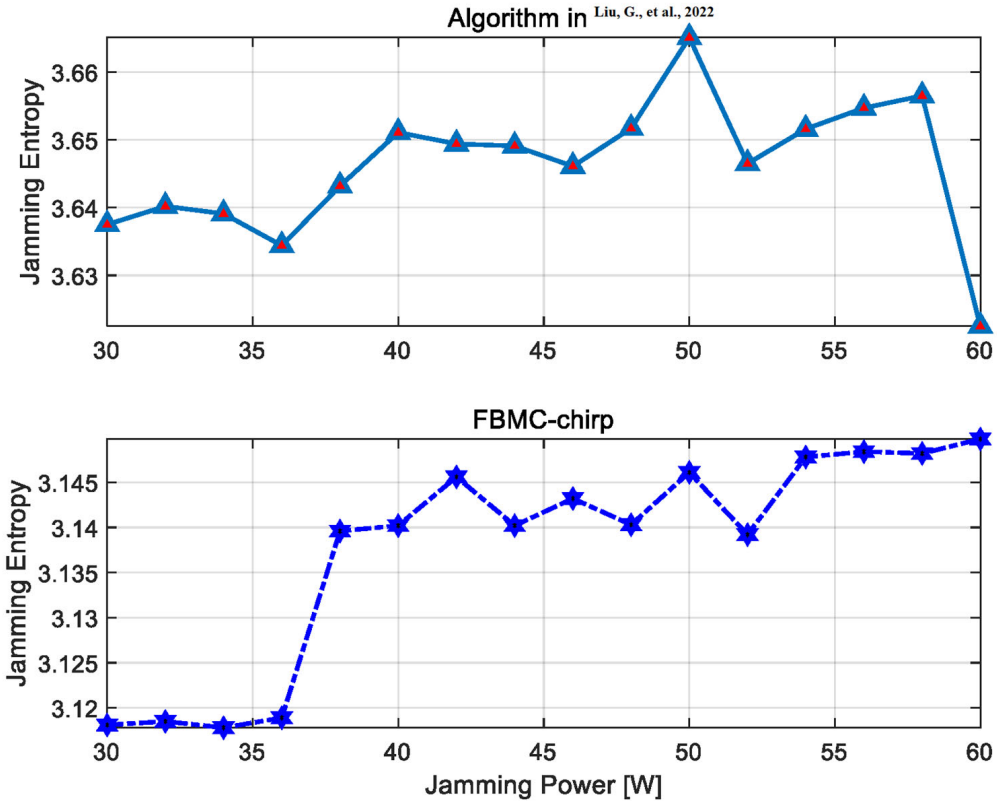

Figure 15. Jamming entropy for the proposed FBMC chirp vs. algorithm in [24]; the number of false targets is 700.

Jamming signal energy mainly affects the jamming signal ratio (JSR). In Figure 16, the JSR gradually increases and saturates as the number of false target jamming increases. When the number of false targets is less than a certain number at the beginning, the JSR level is not high because the jamming effect is not pronounced and the target is not yet covered. Overall, the JSR of our proposed joint waveform based on FBMC chirp is about 20 dB lower than that of the algorithm in [24], requiring less jamming power than traditional chirp or other signals.

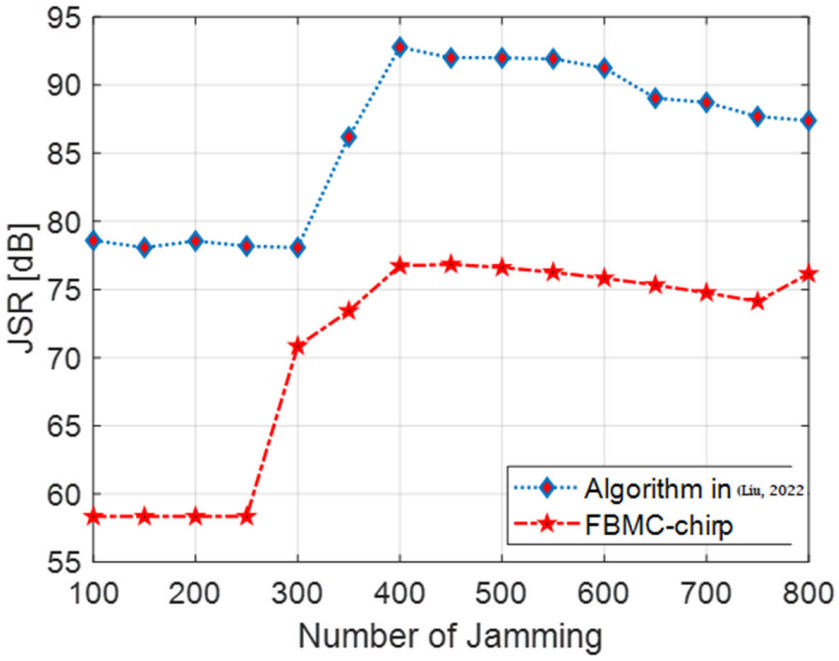

Figure 16. Trade-off between the jamming signal ratio and the number of false targets; SNR = 12 dB [24].

6. Hardware Implementation

The proposed joint communication jamming system was validated on a software-defined radio (SDR) (left image of Figure 17) in a controlled laboratory environment to acquire data and evaluate its radar and communications capabilities. The SDR consists of a single static radar that generates the LFM waveform and performs the basic jammed radar task and a detached communication receiver that simulates the demodulation of the pulse by a friendly communication object. The prototype is highly flexible since all parameters can be set, and the feasibility of the proposed waveform design has been demonstrated. The joint communication jamming platform was placed in the scene (right image in Figure 17) to generate the FBMC chirp waveform, send jamming signals, and perform communication tasks.

The parameters were set as follows: wavelength λ = 3 cm, bandwidth B = 50 MHz, pulse duration τ = 100 µs, N = 3 information bits, G = 3 guard bits per subcarrier, PRF = 1 KHz, and OQAM was the selected modulation scheme. The jamming capability of the joint system was evaluated by calculating the real-time MTD of the pulse received by the SDR. In the acquisition process, when the target moves towards and away from the radar, its range and Doppler characteristics can be observed from the real-time MTD spectrogram (see Figure 18). According to the horizontal coordinate Doppler channel index of 106 in Figure 18a, there were 128 Doppler channels; the target speed was calculated to be 12.422 m/s, and the corresponding speed was 44.719 km/h.

The vertical coordinate indicates the time axis. With the time index of 1.212 µs and the blind area time of 2 µs for the equipment, the moving target position after the near-field blind was about 481.8 m. Considering the near-field blinding error and measurement error, the detection distance error of the SDR was about 3%. As shown in Figure 18b, the MTD result with jamming has completely obscured the moving target.

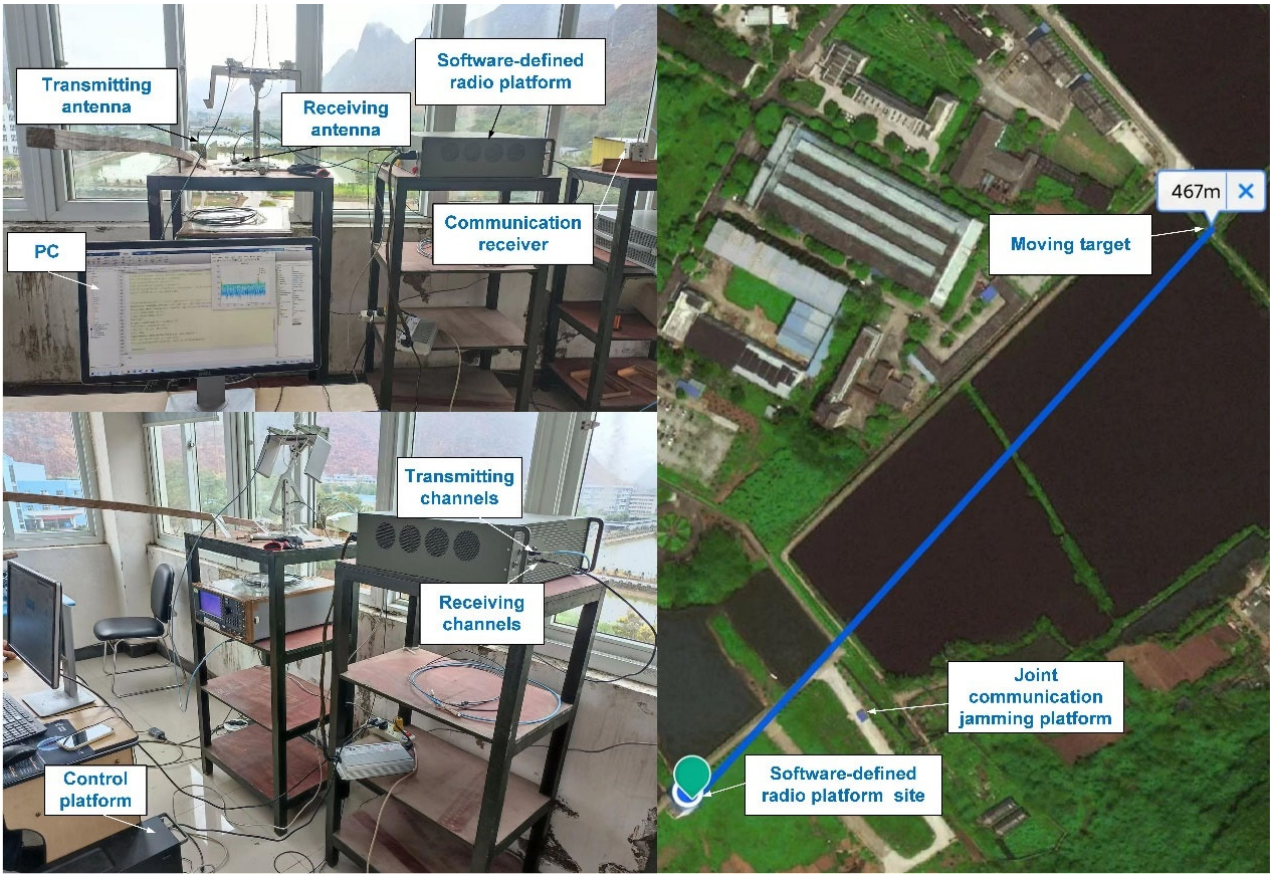

Figure 17. Experimental platform: SDR and spatial position of the experiment.

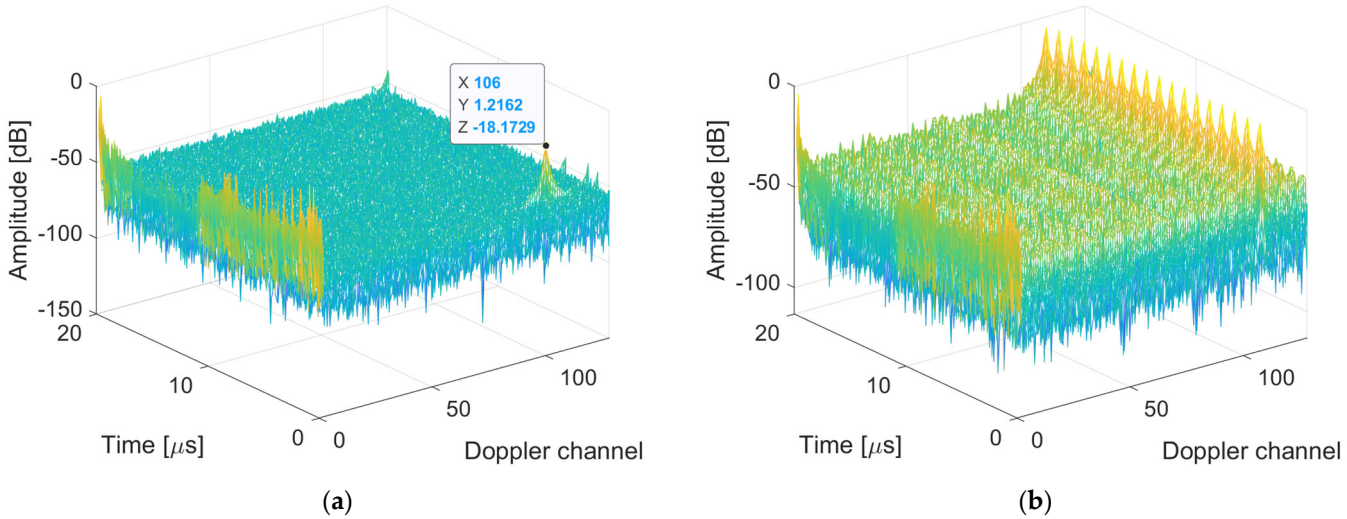

Figure 18. MTD results of target tracking: (**a**) without jamming; (**b**) with jamming.

Furthermore, the SAR imaging simulation of the curve trajectory was completed at the personal computer (PC) end. The jamming echo data received by SDR were superimposed on the SAR imaging echo at the PC end, and the results are shown in Figure 19. Under the influence of jamming, the image's contrast is decreased and the detail information is covered by jamming, leading to multiple false targets in the range dimension.

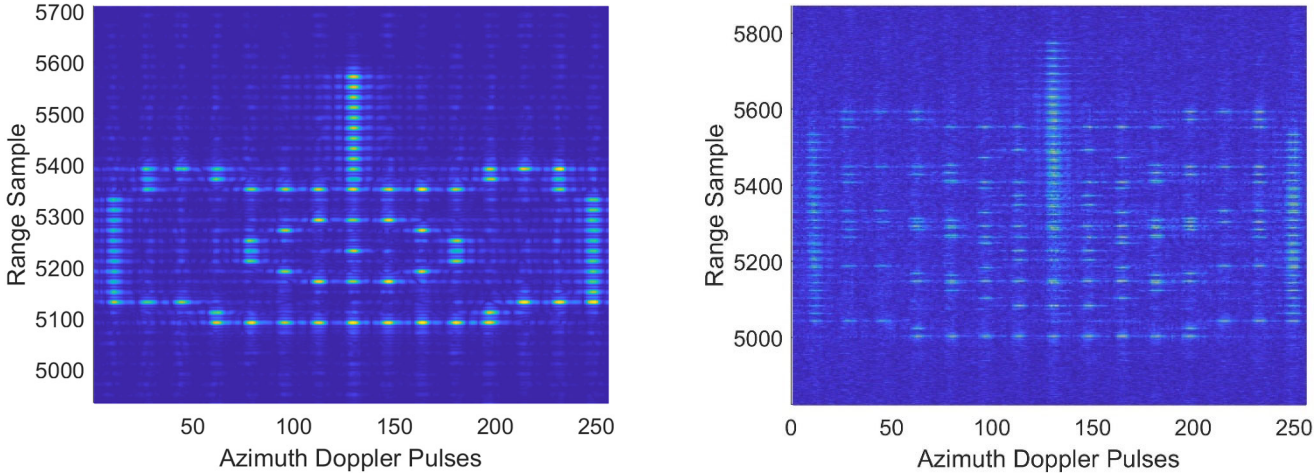

Figure 19. SAR imaging results: (**a**) without jamming; (**b**) SAR jamming result.

7. Conclusions

The FBMC signal uses the prototype pulse to shape the subcarriers, relaxing the requirements for orthogonality. Strict synchronization between the subcarriers is no longer required, and the signal has a higher tolerance for the Doppler frequency offset. FBMC does not use CP to combat multipath effects; instead, OQAM is used to perform independent equalization on subcarriers, achieving a better bit error rate than OFDM used in the communication field. In addition, the good out-of-band suppression of the spectrum and the extremely high spectrum utilization efficiency can make the jamming energy more concentrated in the main lobe and increase the jamming distance. These properties make FBMC a good alternative for a joint communication jamming system.

In this paper, we developed a joint communication jamming waveform based on the FBMC chirp. Modulating the chirp signal to different subcarrier groups can increase the number of false targets in a single pulse period. Since the subcarriers of the FBMC-OQAM signal are orthogonal, the signals are naturally orthogonal. The transmitter and receiver can then be separated to achieve multi-false-target jamming, which can raise the CFAR threshold by about 20 dB and help protect the target from detection.

The ratio of the frequency shift of the designed jamming signal to the modulation frequency depends on the delay time. This makes the designed joint signal more robust in response to jamming and can resist frequency modulation agility. Furthermore, using an intercepted radar signal made it possible to perform channel estimation. Thus, high-speed digital transmission could be achieved while ensuring dense false target jamming. The proposed FBMC chirp joint waveform requires about 20 dB less jamming signal ratio than the existing method, and thus the energy saved can ensure the robust performance of the communication subsystem in the joint communication jamming system. The simulation results show that the joint signal can jam a pulse Doppler radar and excels in communication rate and bit error rate performance, ensuring that instructions are accurately and completely transmitted while implementing effective jamming.

Author Contributions: Conceptualization, G.L. and W.Y.; validation, G.L., W.Y. and Y.B.; formal analysis, W.Y. and Y.W.; investigation, Y.B. and Y.W.; writing—original draft preparation, G.L. and W.Y.; writing—review and editing, G.L., W.Y., Y.B., Y.W. and P.L.; supervision, G.L. and P.L.; project administration, G.L. and P.L.; funding acquisition, G.L. and P.L. All authors have read and agreed to the published version of the manuscript.

Funding: This work was supported by the National Natural Science Foundation of China under Grant Nos. 62171346 and 61805189 and the Natural Science Basic Research Program of Shaanxi (Program No. 2021JM-140).

Data Availability Statement: The data presented in this study are available on request from the corresponding author.

Acknowledgments: The authors are thankful for the academic editor's and reviewers' comments on this work.

Conflicts of Interest: The authors declare no conflict of interest.

References

1. Cohen, D.; Mishra, K.V.; Eldar, Y.C. Spectrum sharing radar: Coexistence via xampling. *IEEE Trans. Aerosp. Electron. Syst.* **2017**, *54*, 1279–1296. [CrossRef]
2. Labib, M.; Reed, J.H.; Martone, A.F.; Zaghloul, A.I. Coexistence between radar and LTE-U systems: Survey on the 5 GHz band. In Proceedings of the 2016 United States National Committee of URSI National Radio Science Meeting (USNC-URSI NRSM), Boulder, CO, USA, 6–9 January 2016; pp. 6–9.
3. Mahal, J.A.; Khawar, A.; Abdelhadi, A.; Clancy, T.C. Spectral coexistence of MIMO radar and MIMO cellular system. *IEEE Trans. Aerosp. Electron. Syst.* **2017**, *53*, 655–668. [CrossRef]
4. Zheng, L.; Lops, M.; Eldar, Y.C.; Wang, X. Radar and communication coexistence: An overview: A Review of Recent Methods. *IEEE Signal Process. Mag.* **2019**, *36*, 85–99. [CrossRef]
5. Hassanien, A.; Amin, M.G.; Zhang, Y.D.; Ahmad, F. Signaling strategies for dual-function radar communications: An overview. *IEEE Aerosp. Electron. Syst. Mag.* **2016**, *31*, 36–45. [CrossRef]
6. Han, L.; Wu, K. Joint wireless communication and radar sensing systems-state of the art and future prospects. *IET Microwaves Antennas Propag.* **2013**, *7*, 876–885. [CrossRef]
7. Blunt, S.D.; Yatham, P.; Stiles, J. Intrapulse radar-embedded communications. *IEEE Trans. Aerosp. Electron. Syst.* **2010**, *46*, 1185–1200. [CrossRef]
8. Ahmed, A.; Zhang, Y.D.; Hassanien, A. Joint radar-communications exploiting optimized OFDM waveforms. *Remote Sens.* **2021**, *13*, 4376. [CrossRef]
9. Zhang, Z.; Nowak, M.J.; Wicks, M.; Wu, Z. Bio-inspired RF steganography via linear chirp radar signals. *IEEE Commun. Mag.* **2016**, *54*, 82–86. [CrossRef]
10. Zhang, Z.; Qu, Y.; Wu, Z.; Nowak, M.J.; Ellinger, J.; Wicks, M.C. RF steganography via LFM chirp radar signals. *IEEE Trans. Aerosp. Electron. Syst.* **2017**, *54*, 1221–1236. [CrossRef]
11. Hassanien, A.; Amin, M.G.; Zhang, Y.D.; Ahmad, F. Phase-modulation based dual-function radar-communications. *IET Radar Sonar Navig.* **2016**, *10*, 1411–1421. [CrossRef]
12. Pappu, C.S.; Beal, A.N.; Flores, B.C. Chaos based frequency modulation for joint monostatic and bistatic radar-communication systems. *Remote Sens.* **2021**, *13*, 4113. [CrossRef]
13. Bekar, M.; Baker, C.J.; Hoare, E.G.; Gashinova, M. Joint MIMO radar and communication system using a PSK-LFM waveform with TDM and CDM approaches. *IEEE Sens. J.* **2021**, *21*, 6115–6124. [CrossRef]
14. Hassanien, A.; Amin, M.G.; Aboutanios, E.; Himed, B. Dual-function radar communication systems: A solution to the spectrum congestion problem. *IEEE Signal Process. Mag.* **2019**, *36*, 115–126. [CrossRef]
15. Banelli, P.; Buzzi, S.; Colavolpe, G.; Modenini, A.; Rusek, F.; Ugolini, A. Modulation formats and waveforms for 5G networks: Who will be the heir of OFDM? An overview of alternative modulation schemes for improved spectral efficiency. *IEEE Signal Process. Mag.* **2014**, *31*, 80–93. [CrossRef]
16. Bellanger, M.G. FBMC Physical Layer: A Primer. PHYDYAS FP7 Project Document. 2010. Available online: http://www.ict-phydyas.org/teamspace/internal-folder/special-session-at-crowncom-2010 (accessed on 5 May 2022).
17. Zhu, K.; Wang, J.; Liang, X.; Wu, Y. Filter bank multicarrier waveform used for integrated SAR and communication systems. *J. Radars* **2018**, *7*, 602–612.
18. Liu, N.; Zhang, Y. A survey of radar ECM and ECCM. *IEEE Trans. Aerosp. Electron. Syst.* **1995**, *31*, 1110–1120.
19. Zou, S.; Jin, X.; Li, L. Airborne AESA radar's ECCM and self-defense jamming analysis. In Proceedings of the 2011 IEEE CIE International Conference on Radar, Chengdu, China, 24–27 October 2011; pp. 1082–1085.
20. Schroer, R. Electronic warfare. [A century of powered flight: 1903–2003]. *IEEE Aerosp. Electron. Syst. Mag.* **2003**, *18*, 49–54. [CrossRef]
21. Deligiannis, A.; Rossetti, G.; Panoui, A.; Lambotharan, S.; Chambers, J.A. Power allocation game between a radar network and multiple jammers. In Proceedings of the 2016 IEEE Radar Conference (RadarConf), Philadelphia, PA, USA, 2–6 May 2016; pp. 1–5.
22. Zhao, D.; Wei, Y.; Liu, Y. Spectrum optimization via FFT-based conjugate gradient method for unimodular sequence design. *Signal Process.* **2018**, *142*, 354–365. [CrossRef]
23. Tang, B.; Liang, J. Efficient algorithms for synthesizing probing waveforms with desired spectral shapes. *IEEE Trans. Aerosp Electron. Syst.* **2019**, *3*, 1174–1189. [CrossRef]
24. Liu, G.; Yang, W.; Wang, Y.; Wang, Z.; Huang, D.; Li, P.; Bao, D.; Man, X.; Wu, B. Joint communication interference system design based on parameter modulation. *Appl. Opt.* **2022**, *61*, 1057–1067. [CrossRef]
25. Sahin, A.; Guvenc, I.; Arslan, H. A survey on multicarrier communications: Prototype filters, lattice structures, and implementation aspects. *IEEE Commun. Surveys Tuts.* **2012**, *16*, 1312–1338. [CrossRef]

26. Liu, G.; Yang, W.; Bao, Y.; Wang, Y.; Li, P.; He, Z. Joint radar communication system design based on filter bank multicarrier modulation scheme. *IET Radar Sonar Navig.* **2023**, *17*, 47–62. [CrossRef]
27. Nam, H.; Choi, M.; Han, S.; Kim, C.; Choi, S.; Hong, D. A new filter-bank multicarrier system with two prototype filters for QAM symbols transmission and reception. *IEEE Trans. Wireless Commun.* **2016**, *15*, 5998–6009. [CrossRef]
28. Kim, C.; Yun, Y.H.; Kim, K.; Seol, J.-Y. Introduction to QAM-FBMC: From waveform optimization to system design. *IEEE Commun. Mag.* **2016**, *54*, 66–73. [CrossRef]
29. Kim, J.H.; Younis, M.; Moreira, A.; Wiesbeck, W. Spaceborne MIMO synthetic aperture radar for multimodal operation. *IEEE Trans. Geosci. Remote Sens.* **2015**, *53*, 2453–2466. [CrossRef]
30. Kim, J.H.; Younis, M.; Moreira, A.; Wiesbeck, W. A novel OFDM chirp waveform scheme for use of multiple transmitters in SAR. *IEEE Trans. Geosci. Remote Sens Lett.* **2013**, *10*, 568–572. [CrossRef]
31. Wang, J.; Liang, X.; Chen, L. MIMO SAR system using digital implemented OFDM waveforms. In Proceedings of the 2012 IEEE International Geoscience and Remote Sensing Symposium (IGARSS), Munich, Germany, 22–27 July 2012; pp. 7428–7431.
32. Fan, W.; Zhou, F.; Tao, M.; Bai, X.; Rong, P.; Yang, S.; Tian, T. Interference mitigation for synthetic aperture radar based on deep residual network. *Remote Sens.* **2019**, *11*, 1654. [CrossRef]
33. Zhou, F.; Zhao, B.; Tao, M.; Bai, X.; Chen, B.; Sun, G. A large scene deceptive jamming method for space-borne SAR. *IEEE Trans. Geosci. Remote Sens.* **2013**, *51*, 4486–4495. [CrossRef]
34. Butt, F.A.; Jalil, M. An overview of electronic warfare in radar systems. In Proceedings of the International Conference on Technological Advances in Electrical, Electronics and Computer Engineering (TAEECE), Konya, Turkey, 9–11 May 2013; pp. 213–217.
35. Shi, L.; Zhou, Y.; Li, D.; Wang, X.; Xiao, S. Multi-false-target jamming effects on the LFM pulsed radar's CFAR detection. *Syst. Eng. Electron.* **2005**, *27*, 818–822.
36. Liu, X.; Li, D. Analysis of cooperative jamming against pulse compression radar based on CFAR. *EURASIP J. Adv. Signal Process.* **2018**, 69. [CrossRef]
37. Weiss, M. Analysis of some modified cell-averaging CFAR processors in multiple target situations. *IEEE Trans. Aerosp. Electron. Syst.* **1982**, *18*, 102–114. [CrossRef]
38. Žáčik, N.; Novák, A.; Soto, A.; Drupka, G. SASS-C processing capability of MSPSR data. *Transport. Res. Procedia* **2017**, *28*, 79–88. [CrossRef]
39. Feichtinger, H.G.; Strohmer, T. *Gabor Analysis and Algorithms: Theory and Applications*; Springer: New York, NY, USA, 2012.
40. Haas, R.; Belfiore, J.-C. A time-frequency well-localized pulse for multiple carrier transmission. *Wireless Pers. Commun.* **1997**, *5*, 1–18. [CrossRef]
41. Bellanger, M.G. Specification and design of a prototype filter for filter bank based multicarrier transmission. In Proceedings of the 2011 IEEE International Conference on Acoustics, Speech, and Signal Processing (ICASSP), Salt Lake City, UT, USA, 7–11 May 2001; pp. 2417–2420.
42. Husam, A. Optimization of FBMC-OQAM Transceiver Architectures. Ph.D. Thesis, Budapest University of Technology and Economics, Budapest, Hungary, 2021.
43. Liu, X.; Li, D.; Hu, R. Research on blanking shift-frequency-multi-carrier jamming against pulse-compression radar based on OS-CFAR. *Acta Armamentarii* **2017**, *38*, 2134–2142. [CrossRef]
44. Liu, X.; Li, D.; Liu, Q. Jamming technique of multiple false targets against linear frequency modulated pulse compression radar based on OS-CFAR. *Syst. Eng. Electron.* **2017**, *39*, 1486–1492.